One Switching Cycle Current Control Strategy for Triple Active Bridge Phase-Shifted DC-DC Converter

Ritwik Chattopadhyay, Sayan Acharya, Ghanshyamsinh Gohil, Subhashish Bhattacharya
FREEDM Systems Centre, North Carolina State Univerity, Raleigh, NC, USA.
Email: rchatto,sachary,gvgohil,sbhatta4@ncsu.edu

***Abstract*—The paper presents two types of one cycle current control method for Triple Active Bridge(TAB) phase-shifted DC-DC converter integrating Renewable Energy Source(RES), Energy Storage System(ESS) and a output dc bus. The main objective of the current control methods is to control the transformer current in each cycle so that dc transients are eliminated during phase angle change from one cycle to the next cycle. In the proposed current control methods, the transformer currents are sampled within a switching cycle and the phase shift angles for the next switching cycle are generated based on sampled current values and current references. The discussed one cycle control methods also provide an inherent power decoupling feature for the three port phase shifted triple active bridge converter. Two different methods, (a) sampling and updating twice in a switching cycle and (b) sampling and updating once in a switching cycle, are explained in this paper. The current control methods are experimentally verified using digital implementation technique on a laboratory made hardware prototype.**

I. Introduction

Integration of Renewable Energy Sources(RES) with Energy Storage Systems(ESS) has been an interesting topic of research[1]-[3]. Large scale integration of RES and ESS requires high efficiency converters. Few of the popular converter architectures for large scale integration have been Cascaded H-Bridge(CHB), Modular Multilevel Converter(MMC) and other multilevel converters[4]-[6]. One of convenient way of integrating RES and ESS is to integrate them using a single DC-DC converter. Transformer isolated bidirectional phase-shifted DC-DC converters have been very popular topic of research over years[7]-[10],[18]-[21] for integration of RES, ESS and load or DC bus. The Dual Active Bridge(DAB) and Triple Active Bridge(TAB) DC-DC converters[7]-[10],[18]-[21] provides few critical advantages like galvanic isolation between different ports, natural Zero Voltage Switching(ZVS) during turn-on which is significant for high frequency switching applications, wide voltage variation in input and output, reduced magnetic components etc. The basic power flow operation of DAB or TAB converter is controlled by controlling the phase-shift angle between different winding voltages. The phase shifted DC-DC converters' control techniques are a key thing for proper operation, which requires the high frequency transformer to operate reliably. Using a conventional PI controller approach for power control or voltage control, the phase angle control method causes saturation during transients in the high frequency transformer. Current control of DAB converter have been proposed in [13]-[14], but the problem of transformer saturation has not been addressed. A peak current control and peak-valley current control for two port DAB converter has been proposed in [15],[16] which controls the transformer winding currents within one switching cycle sampling twice during different switching instants. The methods proposed in [15],[16] use peak current sensing during device switching, which is highly sensitive to noise and EMI generated due to device dv/dt.

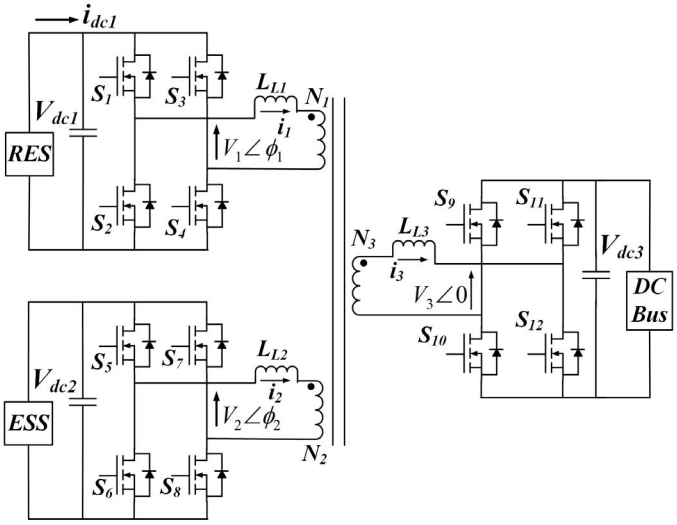

Fig. 1: Triple Active Bridge(TAB) Phase-Shifted DC-DC Converter

In this paper, the current control method discussed in [15],[16] has been extended for three port phase shifted TAB converter, shown in figure 1, using high frequency current sensing method and updating the phase angle. The objective of current control method is to control the high frequency transformer current in each cycle so that dc transients are eliminated from transformer currents during any phase angle change from one cycle to the next. The transformer currents are sensed in each cycle and the phase shift angles for next switching cycle are calculated and updated based on the reference value for next cycle. The control methods discussed in this paper uses two methods for sensing the currents and updating the phase angles. The three port converter of figure 1 has been first proposed in [8], and the power flow among its different ports are coupled to each other. The two current control methods discussed in this paper provide an inherent power decoupling for the three port converter where currents from two ports can be individually controlled. In the first method, the transformer currents are sensed in each half cycle and the phase angles are

978-1-5090-4894-6/17/$31.00 © IEEE

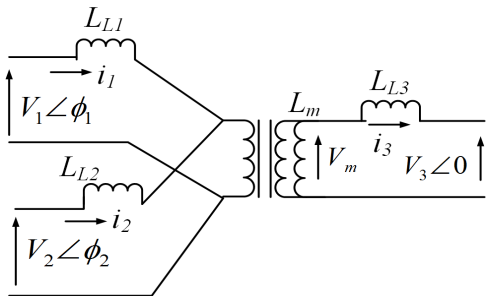

Fig. 2: Equivalent Circuit of Transformer for TAB Converter

updated in the opposite half cycle, which is an extension of the current control method discussed in [15],[16]. In the second method, a new technique is proposed where the transformer currents are sensed and updated once in a switching cycle and they are controlled as per their references in a single cycle. The advantage of the second method is that it allows higher time window to the digital controller for performing other complex calculations and can be implemented for higher frequency applications. The second method also eliminates the error in calculation due to any offset from the high frequency current sensor, which is present in first method for low power cases and it causes the phase angle values and steady state winding currents to oscillate around a stable value. The analysis of the proposed control methods is done in this paper based on the equivalent circuit for three port phase shifted TAB converter, which is shown in figure 2. The current control methods have been experimentally verified and satisfactory results have been obtained for verification. The implementation of the current control techniques have been done using digital controller.

II. Three Port Phase Shifted Converter Analysis

The leakage inductance of high frequency transformer for phase shifted converter acts as energy transferring element[7]. The three H-bridges in figure 1, produce square wave voltages across their respective windings, with phase differences among them, causing active power transfer from one port to the other. The power flow scenarios between the three ports of the transformer of figure 1, are functions of the phase differences between different windings[7]-[10]. In figure 1, the voltage V_3 is considered as the reference voltage and the other two winding voltages V_1,V_2 are are referenced w.r.t. to voltage V_3. The voltages V_1,V_2 have phase shift angles ϕ_1,ϕ_2 which are reference w.r.t. V_3.

The transformer winding currents for a TAB converter are piecewise linear in nature[7]-[10] and are functions of the phase shift angles ϕ_1 and ϕ_2. For this paper work, it is assumed that RES at port 1 act as source and can only deliver power, while the ESS at port 2 can act as both source and sink. Therefore there are three possible scenarios based on the phase shift angles (a) $\phi_1 > \phi_2 > 0$, (b) $\phi_2 > \phi_1 > 0$, and (c) $\phi_1 > 0 > \phi_2$. The three possible cases of winding voltage positions are shown in figures 3-5.

The voltage V_{m1} across the magnetizing inductance L_m, referred to windings 1,2,3 are given in equations (1,2,3). The voltage term V_{xy} refers the voltage V_x referred to winding y.

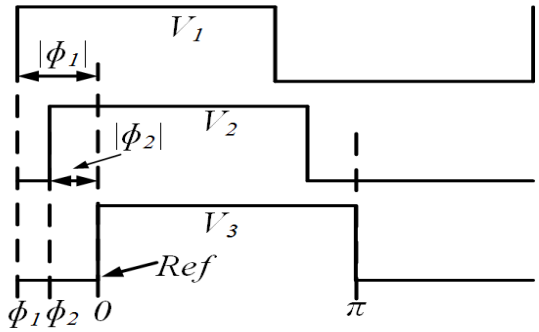

Fig. 3: Mode 1: Winding Voltages when $\phi_1 > \phi_2 > 0$

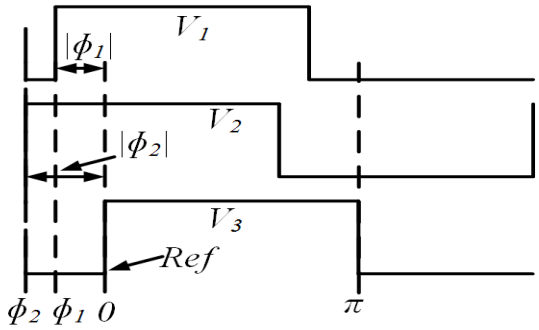

Fig. 4: Mode 2: Winding Voltages when $\phi_2 > \phi_1 > 0$

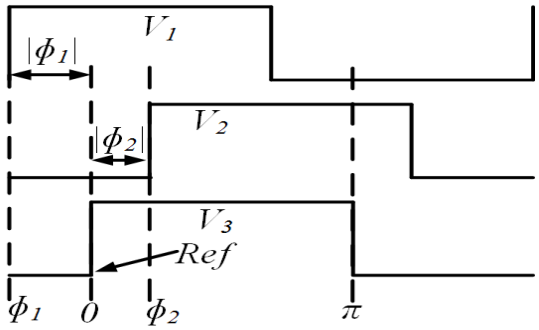

Fig. 5: Mode 3: Winding Voltages when $\phi_1 > 0 > \phi_2$

Similarly, inductance L_{Lxy} refers to inductance L_{Lx} referred to winding y. The piecewise linear nature of transformer winding currents for winding 1,2 and 3 are given in equations (7-9), where $'\theta'_0$ is initial instant for the linear interval x and $'\theta'$ is any instant within that interval x and ${m_x}^y$ is slope of that interval x for current in winding y.

$$V_{m1} = \frac{(V_1 L_{L21} L_{L31} + V_{21} L_{L1} L_{L31} + V_{31} L_{L21} L_{L1}) L_{m1}}{{L_{n1}}^3} \tag{1}$$

$$V_{m2} = \frac{(V_2 L_{L12} L_{L32} + V_{12} L_{L2} L_{L32} + V_{32} L_{L2} L_{L12}) L_{m2}}{{L_{n2}}^3} \tag{2}$$

$$V_{m3} = \frac{(V_{13} L_{L23} L_{L3} + V_{23} L_{L13} L_{L3} + V_3 L_{L23} L_{L13}) L_{m3}}{{L_{n3}}^3} \tag{3}$$

where

$$\begin{aligned} {L_{n1}}^3 = {} & L_{L1} L_{L21} L_{L31} + L_{L1} L_{L21} L_{m1} \\ & + L_{L1} L_{L31} L_{m1} + L_{L21} L_{L31} L_{m1} \end{aligned} \tag{4}$$

$$L_{n2}{}^{3} = L_{L12}L_{L2}L_{L32} + L_{L12}L_{L2}L_{m2} + L_{L12}L_{L32}L_{m2} + L_{L2}L_{L32}L_{m2} \quad (5)$$

$$L_{n3}{}^{3} = L_{L13}L_{L23}L_{L3} + L_{L13}L_{L23}L_{m3} + L_{L13}L_{L3}L_{m3} + L_{L23}L_{L3}L_{m3} \quad (6)$$

$$i_1(\theta) = i_1(\theta_0) + \frac{\{V_1(\theta) - V_{m1}(\theta)\}}{\omega L_{L1}}(\theta - \theta_0) = i_1(\theta_0) + m_x{}^{1}(\theta - \theta_0) \quad (7)$$

$$i_2(\theta) = i_2(\theta_0) + \frac{\{V_{m2}(\theta) - V_2(\theta)\}}{\omega L_{L2}}(\theta - \theta_0) = i_2(\theta_0) + m_x{}^{2}(\theta - \theta_0) \quad (8)$$

$$i_3(\theta) = i_3(\theta_0) + \frac{\{V_{m3}(\theta) - V_3(\theta)\}}{\omega L_{L3}}(\theta - \theta_0) = i_3(\theta_0) + m_x{}^{3}(\theta - \theta_0) \quad (9)$$

The average dc power flow for each port are expressed by product of half cycle average voltage and half cycle average current. The half cycle average voltage is equal to the corresponding dc link voltage for each port for square wave voltage waveform and half cycle average currents are obtained using the equations (7-9). The average dc power flow over a switching cycle for each port are given below. The turns ratio term r_{xy} are defined as $r_{xy} = \frac{N_x}{N_y}$.

$$P_1 = \frac{V_{dc1}r_{13}V_{dc3}\phi_1(\pi - |\phi_1|)L_{L21}L_{L31}}{\pi\omega L_{n1}{}^{3}} + \frac{V_{dc1}r_{12}V_{dc2}(\phi_1 - \phi_2)(\pi - |\phi_1 - \phi_2|)L_{L31}L_{m1}}{\pi\omega L_{n1}{}^{3}} \quad (10)$$

$$P_2 = \frac{V_{dc2}r_{23}V_{dc3}\phi_2(\pi - |\phi_2|)L_{L12}L_{L32}}{\pi\omega L_{n2}{}^{3}} - \frac{r_{21}V_{dc1}V_{dc2}(\phi_1 - \phi_2)(\pi - |\phi_1 - \phi_2|)L_{L32}L_{m2}}{\pi\omega L_{n2}{}^{3}} \quad (11)$$

$$P_3 = \frac{r_{31}V_{dc1}V_{dc3}\phi_1(\pi - |\phi_1|)L_{L23}L_{L3}}{\pi\omega L_{n3}{}^{3}} + \frac{r_{32}V_{dc2}V_{dc3}\phi_2(\pi - |\phi_2|)L_{L13}L_{L3}}{\pi\omega L_{n3}{}^{3}} \quad (12)$$

The above power flow expressions clearly indicate that the systems are coupled to each other and power flow of one port cannot be controlled using one phase angle. The non-linear decoupling method for this has been proposed in [8], but this requires pre-computation of all feasible operating points, and this method does not consider the dynamic phase angle change effects for the triple active bridge converter. Moreover, using this method, the transformer current develops dc transients during phase angle change, which is not addressed in [8]. In the following sections, transformer current control to avoid dc transients during phase change is discussed. The control methods provide inherent power decoupling. In this paper, currents in windings 1 and 3 are controlled which automatically controls the current in winding 2.

III. Triple Active Bridge Converter Current Control

In the current control method, transformer winding currents are sampled in each switching cycle at a fixed instant. The phase shift angles are calculated based on the sampled values and the corresponding reference currents, which are at one switching cycle later at the same instant. Similar current control has been proposed for Dual Active Bridge(DAB) converter in [15],[16] where the transformer winding current is sensed twice and the phase angle is updated twice in a switching cycle. In this paper, the double sampling method has been extended for three port triple active bridge converter and a single sampling method is proposed. The current control for the above TAB converter is implemented here by sensing currents in windings 1 and 3 and updating ϕ_1 and ϕ_2.

A. Double Sampling Method for Current Control

In the double sampling method, the current sampling and phase shift update takes place at the zero and peak of triangular carrier wave, which is used for port 3 gating pulses or winding voltage generation, as shown in figure 6. The reference for the current sample sensed at zero, is at the next zero of carrier i.e., one switching cycle later. The phase angles are calculated within half period of the recent switching cycle and are updated at the next peak of the carrier wave, i.e., at half switching cycle later. Similarly, for the currents sampled at peak of the carrier, the reference is at the next peak and the phase angles are updated in next zero of the carrier wave. From the instantaneous current expressions from (7-9), it can be inferred that the winding currents slopes change for every voltage polarity change. The current control is derived for the scenario of figure 3, and is based on predictive method and the calculated phase angle expressions are same for all scenarios of voltage vectors' positions in figures 3-5. The slopes for the currents i_1 and i_3 are defined in equations (13-18) where $m_x{}^{y}$ is slope for current in winding y in interval x.

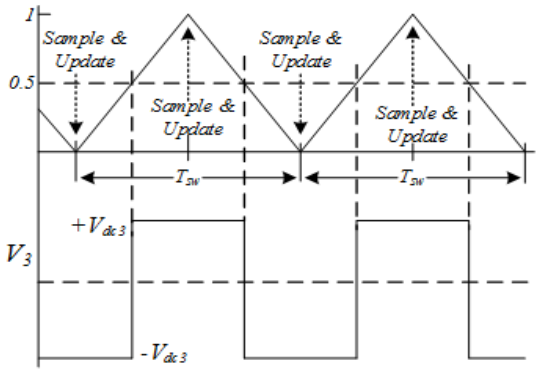

Fig. 6: Sample and Update for Double Sampling Method

During interval $V_1 < 0$, $V_2 < 0$, $V_3 < 0$:

$$m_1{}^{1} = (r_{12}V_{dc2} - V_{dc1})K_1{}^{1} + (r_{13}V_{dc3} - V_{dc1})K_2{}^{1} + r_{13}V_{dc3}K_3{}^{1} \quad (13)$$

$$m_1{}^{3} = (V_{dc3} - r_{31}V_{dc1})K_1{}^{3} + (V_{dc3} - r_{32}V_{dc2})K_2{}^{3} + V_{dc3}K_3{}^{3} \quad (14)$$

During interval $V_1 > 0$, $V_2 < 0$, $V_3 < 0$:

$$m_2{}^1 = (r_{12}V_{dc2} + V_{dc1})K_1{}^1 + (r_{13}V_{dc3} + V_{dc1})K_2{}^1 + r_{13}V_{dc3}K_3{}^1 \quad (15)$$

$$m_2{}^3 = (V_{dc3} + r_{31}V_{dc1})K_1{}^3 + (V_{dc3} - r_{32}V_{dc2})K_2{}^3 + V_{dc3}K_3{}^3 \quad (16)$$

During interval $V_1 > 0$, $V_2 > 0$, $V_3 < 0$:

$$m_3{}^1 = (-r_{12}V_{dc2} + V_{dc1})K_1{}^1 + (r_{13}V_{dc3} + V_{dc1})K_2{}^1 + r_{13}V_{dc3}K_3{}^1 \quad (17)$$

$$m_3{}^3 = (V_{dc3} + r_{31}V_{dc1})K_1{}^3 + (V_{dc3} + r_{32}V_{dc2})K_2{}^3 + V_{dc3}K_3{}^3 \quad (18)$$

$$K_1{}^1 = \frac{L_{L31}L_{m1}}{\omega L_{n1}{}^3} \quad (19) \qquad K_2{}^1 = \frac{L_{L21}L_{m1}}{\omega L_{n1}{}^3} \quad (20)$$

$$K_3{}^1 = \frac{L_{L31}L_{L21}}{\omega L_{n1}{}^3} \quad (21) \qquad K_1{}^3 = \frac{L_{m3}L_{L23}}{\omega L_{n3}{}^3} \quad (22)$$

$$K_2{}^3 = \frac{L_{m3}L_{L13}}{\omega L_{n3}{}^3} \quad (23) \qquad K_3{}^3 = \frac{L_{L13}L_{L23}}{\omega L_{n3}{}^3} \quad (24)$$

The sample and update instants are shown in figure 7, i_1 and i_3 are sampled at the midpoint instant of the output winding voltage V_3 during both positive and negative half cycles, i.e. when the carrier of figure 7 reaches zero and peak. The reference for any current sample are at one switching cycle later. The predictive control algorithm works in the manner that it samples at zero and peak of the carrier wave for V_3, calculates the new phase shift angle values ϕ_1 and ϕ_2, and updates the PWM generator at half switching cycle later. From figure 7, during positive half cycle, the controller samples at $(n-1)^{th}$ sampling instant while the reference is at $(n+1)^{th}$ sampling instant, and the PWM phase shift generator is updated at n^{th} sampling instant. Similarly, for negative half cycle, the controller samples at n^{th} sampling instant, the reference is at $(n+2)^{th}$ sampling instant, and the new phase shift angles ϕ_1 and ϕ_2 are updated into the PWM generator at $(n+1)^{th}$ sampling instant. The predictive controller uses the sampled winding currents values and calculates the phase shift angles based on previous half switching cycle values of phase shift angles. The controller updates the PWM generator with new phase shift values at the midpoint of positive and negative polarity of winding voltage V_3.

From figure 7, starting from $(n-1)^{th}$ sampling instant, the winding 1 and 3 currents at $(n+1)^{th}$ sampling instant can be expressed using current slopes based on piecewise linear model of equations (7-9) and (13-18).

$$i_{1\_ref} = i_{1sam(n+1)} = i_{1sam(n-1)} - m_1{}^1(\frac{\pi}{2} - \phi_1{}^{n-1}) - m_2{}^1(\phi_1{}^{n-1} - \phi_2{}^{n-1}) - m_3{}^1(\phi_2{}^{n-1}) + m_1{}^1(\pi - \phi_1{}^n) + m_2{}^1(\phi_1{}^n - \phi_2{}^n) + m_3{}^1(\phi_2{}^n) - m_1{}^1(\frac{\pi}{2}) \quad (25)$$

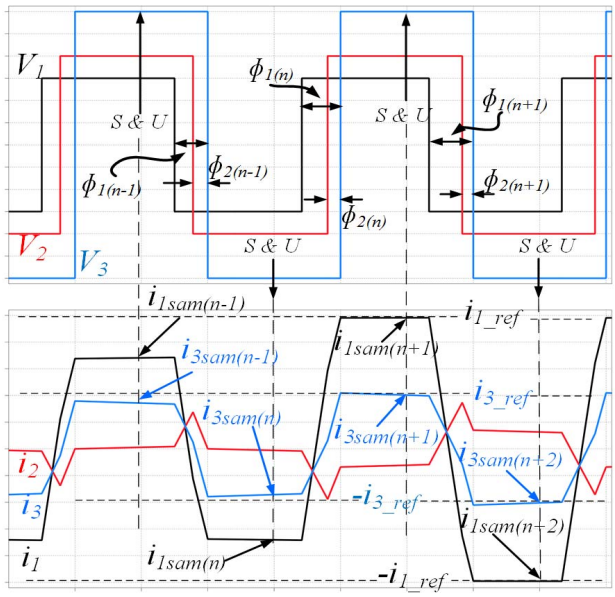

Fig. 7: Current Control Action using Double Sampling Method

$$i_{3\_ref} = i_{3sam(n+1)} = i_{3sam(n-1)} - m_1{}^3(\frac{\pi}{2} - \phi_1{}^{n-1}) - m_2{}^3(\phi_1{}^{n-1} - \phi_2{}^{n-1}) - m_3{}^3(\phi_2{}^{n-1}) + m_1{}^3(\pi - \phi_1{}^n) + m_2{}^3(\phi_1{}^n - \phi_2{}^n) + m_3{}^3(\phi_2{}^n) - m_1{}^3(\frac{\pi}{2}) \quad (26)$$

Rearranging equations (25)-(26), the following matrix form is generated.

$$\begin{bmatrix} (m_2{}^1 - m_1{}^1) & (m_3{}^1 - m_2{}^1) \\ (m_2{}^3 - m_1{}^3) & (m_3{}^1 - m_2{}^3) \end{bmatrix} \begin{bmatrix} \phi_1{}^n \\ \phi_2{}^n \end{bmatrix} = \begin{bmatrix} J_1 \\ J_2 \end{bmatrix} \quad (27)$$

where

$$J_1 = (i_{1\_ref} - i_{1sam(n-1)}) + (m_2{}^1 - m_1{}^1)\phi_1{}^{n-1} + (m_3{}^1 - m_2{}^1)\phi_2{}^{n-1} \quad (28)$$

$$J_2 = (i_{3\_ref} - i_{3sam(n-1)}) + (m_2{}^3 - m_1{}^3)\phi_1{}^{n-1} + (m_3{}^3 - m_2{}^3)\phi_2{}^{n-1} \quad (29)$$

The matrix elements are expressed in terms of circuit parameters as given below.

$$m_2{}^1 - m_1{}^1 = 2V_{dc1}(K_1{}^1 + K_2{}^1 + K_3{}^1) \quad (30)$$

$$m_3{}^1 - m_2{}^1 = -2r_{12}V_{dc2}K_1{}^1 \quad (31)$$

$$m_2{}^3 - m_1{}^3 = 2r_{31}V_{dc1}K_1{}^3 \quad (32)$$

$$m_3{}^3 - m_2{}^3 = 2r_{32}V_{dc2}K_2{}^3 \quad (33)$$

Solving the equation (26), the required phase angles to be updated for n^{th} sampling instant are obtained as follows.

$$\begin{bmatrix} \phi_1{}^n \\ \phi_2{}^n \end{bmatrix} = \begin{bmatrix} 2r_{32}V_{dc2}K_2{}^3 & 2r_{12}V_{dc2}K_1{}^1 \\ -2r_{31}V_{dc1}K_1{}^3 & 2V_{dc1}(K_1{}^1 + K_2{}^1 + K_3{}^1) \end{bmatrix} \times \begin{bmatrix} J_1 \\ J_2 \end{bmatrix} \times \frac{1}{D} \quad (34)$$

where

$$D = 4r_{32}V_{dc1}V_{dc2}K_2{}^3(K_1{}^1 + K_2{}^1 + K_3{}^1) + 4r_{31}r_{12}V_{dc1}V_{dc2}K_1{}^3K_1{}^1 \quad (35)$$

Expanding equations (34)-(35), the following solutions for the phase angles are obtained.

$$\phi_1{}^n = \phi_1{}^{n-1} + \frac{\Delta i_{1ref}(2r_{32}V_{dc2}K_2{}^c)}{D} + \frac{\Delta i_{3ref}(2r_{12}V_{dc2}K_1{}^1)}{D} \tag{36}$$

$$\phi_2{}^n = \phi_2{}^{n-1} + \frac{\Delta i_{1ref}(-2r_{31}V_{dc1}K_1{}^3)}{D} + \frac{\Delta i_{3ref}(2V_{dc1}(K_1{}^1 + K_2{}^1 + K_3{}^1))}{D} \tag{37}$$

where

$$\Delta i_{1ref} = (i_{1\_ref} - i_{1sam(n-1)}) \tag{38}$$

$$\Delta i_{3ref} = (i_{3\_ref} - i_{3sam(n-1)}) \tag{39}$$

For the negative half cycle also, the same equations applies, only Δi_{1ref} and Δi_{3ref} change as given below.

$$\phi_1{}^{n+1} = \phi_1{}^n + \frac{\Delta i_{1ref}(2r_{32}V_{dc2}K_2{}^3)}{D} + \frac{\Delta i_{3ref}(2r_{12}V_{dc2}K_1{}^1)}{D} \tag{40}$$

$$\phi_2{}^{n+1} = \phi_2{}^n + \frac{\Delta i_{1ref}(-2r_{31}V_{dc1}K_1{}^3)}{D} + \frac{\Delta i_{3ref}(2V_{dc1}(K_1{}^1 + K_2{}^1 + K_3{}^1))}{D} \tag{41}$$

where

$$\Delta i_{1ref} = (-i_{1\_ref} - i_{1sam(n)}) \tag{42}$$

$$\Delta i_{3ref} = (-i_{3\_ref} - i_{3sam(n)}) \tag{43}$$

The equations (36-43) define the current predictive control of triple active bridge converter using double sampling of winding currents. The above method has been derived using the case when both the winding voltages V_1 and V_2 lead V_3, however the derived expressions can still be applied for any of the possible lead-lag cases of winding voltages defined in figures (3-5).

B. Single Sampling Method for Current Control

In the single sampling method, the current sampling and phase shift update takes place only at the zero of triangular carrier wave for voltage V_3, as shown in figure 8. The references for the currents i_1 and i_3 are at the zero and peak of the carrier. The single sample and update method proposed here makes sure that during the peak and zero of the carrier wave, the winding currents reach their reference values. The single sampling method for thriple active bridge converter is explained in figure 9. Here during negative to positive transition of voltages, the phase angles are defined as $\phi_{1(u)}$ and $\phi_{2(u)}$. Similarly, during negative to positive transition of voltages, the phase angles are defined as $\phi_{1(d)}$ and $\phi_{2(d)}$.

$$i_{1\_ref} = i_{1sam(n)} + m_1{}^1(\frac{\pi}{2} - \phi_{1u(n)}) + m_2{}^1(\phi_{1u(n)} - \phi_{2u(n)}) + m_3{}^1\phi_{2u(n)} - m_1{}^1\frac{\pi}{2} \tag{44}$$

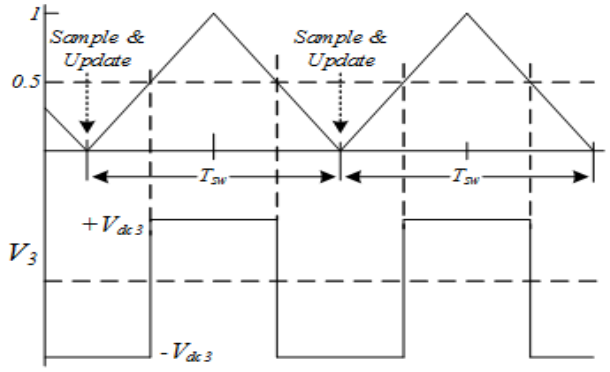

Fig. 8: Sample and Update for Single Sampling Method

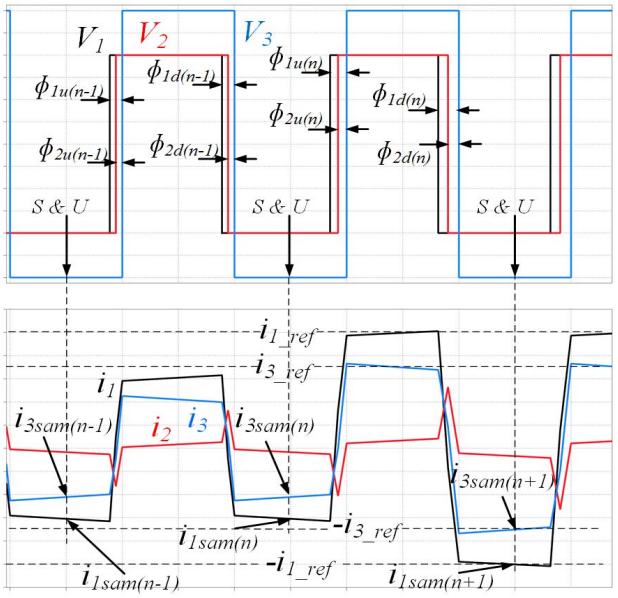

Fig. 9: Current Control Action using Single Sampling Method

$$i_{3\_ref} = i_{3sam(n)} + m_1{}^3(\frac{\pi}{2} - \phi_{1u(n)}) + m_2{}^3(\phi_{1u(n)} - \phi_{2u(n)}) + m_3{}^3\phi_{2u(n)} - m_1{}^1\frac{\pi}{2} \tag{45}$$

$$\begin{aligned} i_{1sam(n)} &= i_{1sam(n-1)} + m_1{}^1(\frac{\pi}{2} - \phi_{1u(n-1)}) \\ &+ m_2{}^1(\phi_{1u(n-1)} - \phi_{2u(n-1)}) + m_3{}^1\phi_{2u(n-1)} \\ &- m_1{}^1(\pi - \phi_{1d(n-1)}) - m_2{}^1(\phi_{1d(n-1)} - \phi_{2d(n-1)}) \\ &- m_3{}^1\phi_{2d(n-1)} + m_1{}^1\frac{\pi}{2} \end{aligned} \tag{46}$$

$$\begin{aligned} i_{3sam(n)} &= i_{3sam(n-1)} + m_1{}^3(\frac{\pi}{2} - \phi_{1u(n-1)}) \\ &+ m_2{}^3(\phi_{1u(n-1)} - \phi_{2u(n-1)}) + m_3{}^3\phi_{2u(n-1)} \\ &- m_1{}^3(\pi - \phi_{1d(n-1)}) - m_2{}^3(\phi_{1d(n-1)} - \phi_{2d(n-1)}) \\ &- m_3{}^3\phi_{2d(n-1)} + m_1{}^3\frac{\pi}{2} \end{aligned} \tag{47}$$

Using the equations (46),(47) in place of $i_{1sam(n)}$,$i_{2sam(n)}$ in equations (44),(45) a matrix similar to equation (27) is

obtained. Repeating the steps in equations (27) to (35), the following expressions for $\phi_{1u(n)}$ and $\phi_{2u(n)}$ are obtained.

$$\phi_{1u(n)} = \phi_{1d(n-1)} - \phi_{1u(n-1)} + \frac{\Delta i_{1ref}(2r_{32}V_{dc2}{K_2}^3)}{D} + \frac{\Delta i_{3ref}(2r_{12}V_{dc2}{K_1}^1)}{D} \quad (48)$$

$$\phi_{2u(n)} = \phi_{2d(n-1)} - \phi_{2u(n-1)} + \frac{\Delta i_{1ref}(-2r_{31}V_{dc1}{K_1}^3)}{D} + \frac{\Delta i_{3ref}(2V_{dc1}({K_1}^1 + {K_2}^1 + {K_3}^1))}{D} \quad (49)$$

where

$$\Delta i_{1ref} = (i_{1\_ref} - i_{1sam(n)}) \quad (50)$$

$$\Delta i_{3ref} = (i_{3\_ref} - i_{3sam(n)}) \quad (51)$$

The phase shift angles $\phi_{1d(n)}$ and $\phi_{2d(n)}$ are calculated below.

$$-i_{1\_ref} = i_{1sam(n)} + {m_1}^1(\frac{\pi}{2} - \phi_{1u(n)}) + {m_2}^1(\phi_{1u(n)} - \phi_{2u(n)}) + {m_3}^1\phi_{2u(n)} - {m_1}^1(\pi - \phi_{1d(n)}) - {m_2}^1(\phi_{1d(n)} - \phi_{2d(n)}) - {m_3}^1(\phi_{2d(n)}) + {m_1}^1\frac{\pi}{2} \quad (52)$$

$$-i_{3\_ref} = i_{3sam(n)} + {m_1}^3(\frac{\pi}{2} - \phi_{1u(n)}) + {m_2}^3(\phi_{1u(n)} - \phi_{2u(n)}) + {m_3}^3\phi_{2u(n)} - {m_1}^3(\pi - \phi_{1d(n)}) - {m_2}^3(\phi_{1d(n)} - \phi_{2d(n)}) - {m_3}^3(\phi_{2d(n)}) + {m_1}^3\frac{\pi}{2} \quad (53)$$

Using the equations (44),(45) in places of $i_{1sam(n)}$ and $i_{3sam(n)}$ in equations (52),(53) the following expressions for $\phi_{1d(n)}$ and $\phi_{2d(n)}$ are obtained.

$$\phi_{1d(n)} = \frac{2i_{1ref}(2r_{32}V_{dc2}{K_2}^3) + 2i_{cref}(2r_{12}V_{dc2}{K_1}^1)}{D} \quad (54)$$

$$\phi_{2d(n)} = \frac{4i_{1ref}r_{31}V_{dc1}{K_1}^3}{D} + \frac{4i_{cref}V_{dc1}({K_1}^1 + {K_1}^2 + {K_1}^3)}{D} \quad (55)$$

The derived equations (48-51) and (54-55) define the current control using single sampling methods to control the transformer current in each cycle. The current control equations have been derived using the case for voltage vectors' positions for $\phi_1 > \phi_2 > 0$ case(figure 3), but the same set of equations are applicable to other two cases of $\phi_2 > \phi_1 > 0$ and $\phi_1 > 0 > \phi_2$, shown in figures 4 and 5. The current control equations have also been derived for the other two cases of figures 4 and 5, and the derived phase angle expressions for ϕ_1 and ϕ_2 have been found to be same for all the cases. Hence, change in voltage vectors' positions from any of the cases in figures (3-5) to any of the other two cases can be achieved using the same equations for ϕ_1 and ϕ_2.

IV. Experimental Study for Current Control

The aforementioned current control methods have been implemented in a laboratory scale hardware prototype using a three port transformer with 1:1:1.5 turns ratio. The hardware prototype has three H-bridges built using SiC Mosfets. The experimental study has been carried out at lower dc bus voltages, 200V for V_{dc1}, V_{dc2} and 300V for V_{dc3}. The high frequency transformer has been made using ferrite material 3C97 and windings are made using litz wire. Figure 10 shows the high frequency transformer used for experimental study. The transformer details are given in table 1. Figure 11 shows the 2MHz bandwidth Sensitec current sensor CMS3025ABA used for sensing high frequency transformer currents.

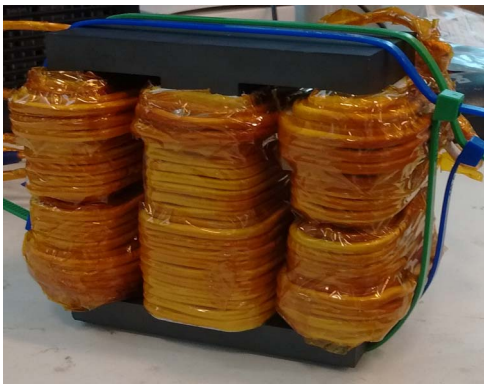

Fig. 10: Three Port High Frequency Transformer

TABLE I: Transformer Details

Leakage inductance L_{L1}	80μH
Leakage inductance L_{L2}	110μH
Leakage inductance L_{L3}	150μH
Magnetizing inductance L_m	9.17mH
Number of turns N_1	22
Number of turns N_2	22
Number of turns N_3	33
Switching Frequency f_s	25kHz

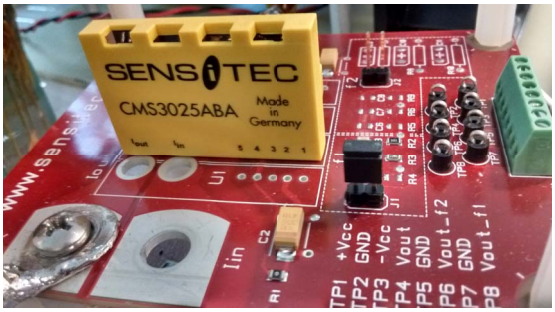

Fig. 11: High Frequency Current Sensor

The closed loop operation is performed by performing a dc voltage control at the output port at 300V and controlling the transformer winding currents. The block diagram for the closed loop control is shown in figure 12. The outer voltage loop generates the i_{3ref}, which is reference for the output port high frequency current i_3. The current reference i_{1ref}, which is reference for port 1 high frequency current i_1, can be generated from MPPT controller or from other current reference generator. For the experimental purpose in this purpose, the i_{1ref} has been fed externally into the controller. The controller used for the aforementioned current control methods is TI DSP TMS320F28335 with 150MHz clock.

978-1-5090-4894-6/17/$31.00 © IEEE

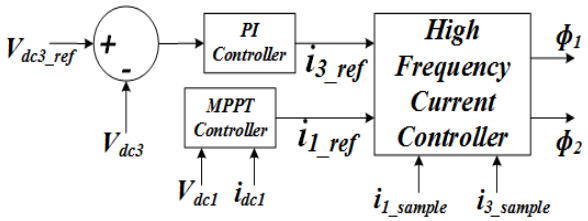

Fig. 12: Closed Loop Control for Three Port Converter

The current control is verified in the hardware prototype by using a step change in the current reference i_{1ref}. The experimental results for double sampling method are shown in figures 13 and 14, where it can be observed that the Sample & Update (S&U) action signal occurs twice in a switching cycle. Figure 13 shows the transient change in current waveforms during a step change decrease in i_{1ref}. As the control signal CS goes high at t_1, the i_{1ref} changes to a new value and the controller calculates the new phase shift angles for positive half cycle references before the next S&U instant t_2. The controller updates the new values for ϕ_1 and ϕ_2 at t_2 and samples the negative half cycle current samples. The positive half cycle i_1 change is reflected at t_3 when i_1 reaches the new reference at t_3. The new phase angles values for ϕ_1 and ϕ_2 in negative half cycle are calculated between t_2 and t_3 to control the current values as per the reference in negative half cycle. The new phase angle values for ϕ_1 and ϕ_2 are updated at t_3. The negative half cycle value for i_1 reaches the reference at t_4. Using this technique, the i_1 settles at new reference value in both positive and negative half cycle within one switching cycle. As $V_{dc3-ref}$ does not change, i_{3ref} also does not change and the controller maintains the current at the same reference value. The port 2 current i_2 changes automatically to new value to show the reflected change in power level. Figure 14 shows the V_{dc3} control and i_{1ref} control when the reference for i_1 goes high at t_1. The controller performs similar control actions in this case as in figure 13, to control i_1 and i_3 as per the new references and maintains the output voltage V_{dc3}.

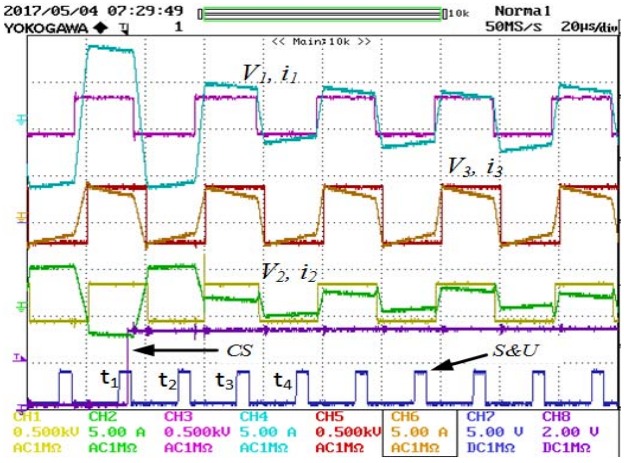

Fig. 13: Transformer Current Control Using Double Sampling

The single sampling method control results are shown in figures 15 and 16. In the figures 15 and 16, it can be observed

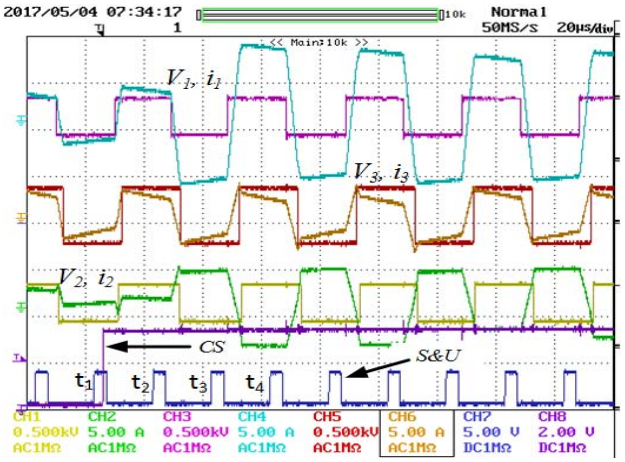

Fig. 14: Transformer Current Control Using Double Sampling

that the S&U pulses occur once in a switching cycle. Figure 15 shows the transient change in current waveforms during a step change increase in i_{1ref}. As the control signal CS goes high at t_1, the i_{1ref} changes to a new value and the controller calculates the new values for phase shift angles ϕ_1, ϕ_2 between t_1 and t_2. The controller updates the new values of $\phi_{1(u)}$, $\phi_{2(u)}$,$\phi_{1(d)}$ and $\phi_{2(d)}$ into PWM controller at t_2 for during the positive half cycle transition and negative half cycle transition. The changes in transformer currents are reflected during the switching cycle between t_3 and t_2. The transformer currents reach their new references for both positive and negative half cycle within one switching cycle. The current i_3 reflects no change, as no change in $V_{dc3-ref}$ occurs or any loading condition is changed. As a result, the current i_2 changes to take in the extra power for the extra power fed in by port 1. The current control result shown in figure 16 takes place in a similar manner as in figure 15, where the current reference port 1 decreases by a step change. The controller performs the same series of actions to control the transformer winding currents in one switching cycle.

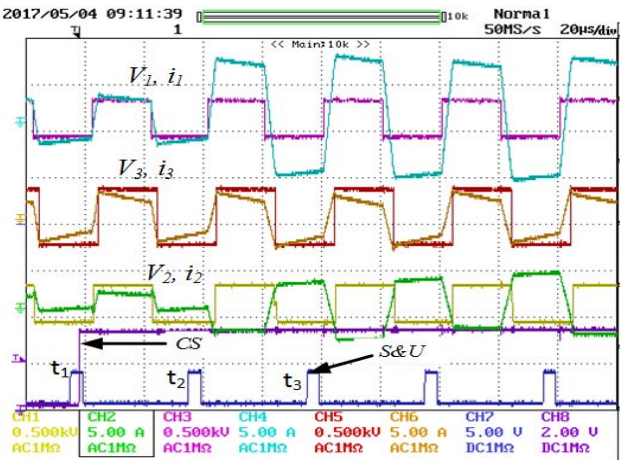

Fig. 15: Transformer Current Control Using Single Sampling

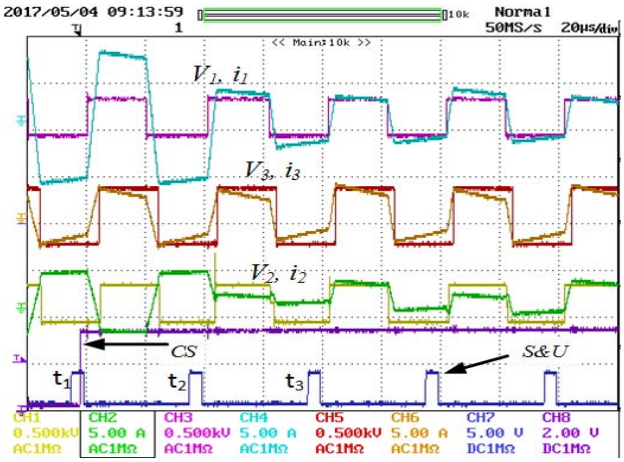

Fig. 16: Transformer Current Control Using Single Sampling

V. Conclusion

The aforementioned current control methods for the three port phase-shifted converter using double sampling and single sampling techniques have worked successfully to control the transformer winding currents in its alternating shape from cycle to cycle, while eliminating high dc transients from the winding currents. The current control methods also provide a natural decoupling of power flow from the phase angle derivation explained in section 3. The double sampling method requires fast processor for performing all the calculations before the next sample and update instant. The single sampling method can work using a comparatively slower controller and it offers more time window in a switching cycle to the controller to perform other control actions if necessary. For low power conditions, when winding currents are low, the double sampling method creates an oscillation in calculated values of phase angles and resulting transformer currents, which occurs due to dc offset of sensor output. This oscillation has been found to be absent using single sampling method. Overall, the proposed control methods work satisfactorily to control transformer winding currents in a cycle by cycle manner.

References

[1] G.J. Tsekouras, F.D. Kanellos; J. Prousalidis,"Simplified method for the assessment of ship electric power systems operation cost reduction from energy storage and renewable energy sources integration,"*IET Electrical Systems in Transportation*, 2015, vol. 5, Issue. 2, pp. 61-69.

[2] H. Su, A.E. Gamal,"Modeling and Analysis of the Role of Energy Storage for Renewable Integration: Power Balancing," *IEEE Tran. on Power Systems*, 2013, vol. 28, Issue. 4, pp. 4109-4117.

[3] H. Xie, S. Zheng, M. Ni,"Microgrid Development in China: A method for renewable energy and energy storage capacity configuration in a megawatt-level isolated microgrid" *IEEE Electrification Magazine*, 2017, vol. 5, Issue. 2, pp.28-35.

[4] C.D. Townsend, Y. Yu, G. Konstantinou, V.G. Agelidis,"Cascaded H-Bridge Multilevel PV Topology for Alleviation of Per-Phase Power Imbalances and Reduction of Second Harmonic Voltage Ripple,"*IEEE Tran. on Power Electronics*, 2016, vol. 31, Issue. 8, pp. 5574-5586.

[5] F. Rong, X. Gong, S. Huang,"A Novel Grid-Connected PV System Based on MMC to Get the Maximum Power Under Partial Shading Conditions,"*IEEE Tran. on Power Electronics*, 2017, vol. 32, Issue. 6, pp. 4320-4333.

[6] M.S. Manoharan, A. Ahmed, J.H. Park,"A PV Power Conditioning System Using Nonregenerative Single-Sourced Trinary Asymmetric Multilevel Inverter With Hybrid Control Scheme and Reduced Leakage Current,"*IEEE Trans. on Power Electronics*, 2017, vol. 21, Issue. 10, pp. 7602-7614.

[7] M.N. Kheraluwala, R.W. Gascoigne, D.M. Divan, E.D. Baumann,"Performance characterization of a high-power dual active bridge DC-to-DC converter,"*IEEE Trans. on Ind. Appl.*, 1992, vol. 28, Issue. 6, pp. 1294-1301.

[8] C. Zhao, S.D. Round, J.W. Kolar, "An Isolated Three-Port Bidirectional DC-DC Converter With Decoupled Power Flow Management," *IEEE Trans. on Power Elect.*, 2008, vol. 23, Issue. 5, pp. 2443-2443.

[9] F. Krismer, J.W. Kolar,"Efficiency-Optimized High-Current Dual Active Bridge Converter for Automotive Applications,"*IEEE Trans. on Ind. Elect.*, 2012, vol. 59, Issue. 7, pp. 2745-2760.

[10] Y. Yu, K. Masumoto, K. Wada, Y. Kado,"Power flow control of a triple active bridge DC-DC converter using GaN power devices for a low-voltage DC power distribution system,"*in proc. IEEE 3rd International Future Energy Electronics Conference and ECCE Asia (IFEEC 2017 - ECCE Asia)*, 2017, pp. 772-777.

[11] R. Chattopadhyay, S. Bhattacharya, "Modular isolated DC-DC converter with multi-limb transformer for interfacing of renewable energy sources," in *proc. IEEE Applied Power Electronics Conference and Exposition (APEC)*, 2015, pp. 3039-3046.

[12] R. Chattopadhyay, G. Gohil, S. Bhattacharya, "Split-winding Type Three Limb Core Structured HF transformer for Integrating PV and Energy Storage(ES)," in *proc. IEEE Applied Power Electronics Conference and Exposition (APEC)*, 2017, pp. 2997-3004.

[13] S.P. Engel, N. Soltau, H. Stagge, R.W. De Doncker, "Dynamic and Balanced Control of Three-Phase High-Power Dual-Active Bridge DCDC Converters in DC-Grid Applications," *IEEE Trans. on Power Electronics*, 2013, vol. 28, Issue. 4, pp. 1880-1889.

[14] S.P. Engel, N. Soltau, H. Stagge, R.W. De Doncker, "Improved Instantaneous Current Control for High-Power Three-Phase Dual-Active Bridge DCDC Converters," *IEEE Trans. on Power Electronics*, 2014, vol. 29, Issue. 8, pp. 4067-4077.

[15] S. Dutta, S. Hazra, S. Bhattacharya, "A Digital Predictive Current-Mode Controller for a Single-Phase High-Frequency Transformer-Isolated Dual-Active Bridge DC-to-DC Converter," *IEEE Trans. on Ind. Elec.*, 2016, vol. 63, Issue. 9, pp. 5943-5952.

[16] J. Huang, Y. Wang, Z. Li, W. Lei, "Predictive valley-peak current control of isolated bidirectional dual active bridge DC-DC converter," in *proc. IEEE Energy Conversion Congress and Exposition (ECCE)*, 2015, pp. 1467-1472.

[17] Y. Panov, M.M. Jovanovi, B.T. Irving, "Novel transformer-flux-balancing control of dual-active-bridge bidirectional converters," *in proc. IEEE 2015 Annual Applied Power Electronics Conference and Exposition(APEC),* 2015, pp. 42-49.

[18] R. Chattopadhyay, S. Bhattacharya, "Decoupled power flow using phase shift control and ZVS cases for a three limb high frequency transformer based three-port DAB integrating PV and energy storage," *IEEE Industry Applications Society Annual Meeting*, 2016, pp. 1-8.

[19] R. Chattopadhyay, S. Bhattacharya, "ZVS analysis and power flow control for three limb transformer enabled SiC Mosfet based three port DAB integrating PV and Energy Storage(ES)," in *proc. IEEE Energy Conversion Congress and Exposition (ECCE)*, 2016, pp. 1-8.

[20] R. Chattopadhyay, S. Bhattacharya, "Power flow control and ZVS analysis of three limb high frequency transformer based three-port DAB," in *proc. IEEE Applied Power Electronics Conference and Exposition (APEC)*, 2016, pp. 778-785.

[21] R. Chattopadhyay, M.A. Juds, P.R. Ohodnicki, S. Bhattacharya, "Modelling, design and analysis of three limb high frequency transformer including transformer parasitics, for SiC Mosfet based three port DAB," in *proc. 42nd Annual Conference of the IEEE Industrial Electronics Societ(IECON)*, 2016, pp. 4181-4186.